On the Initiation of Upward Negative Lightning by Nearby Lightning Activity: An Analytical Approach

Antonio Sunjerga[1], Marcos Rubinstein[2], Farhad Rachidi[1], Vernon Cooray[3]

[1] Electromagnetic Compatibility Laboratory, Swiss Federal Institute of Technology (EPFL), 1015 Lausanne, Switzerland
[2] University of Applied Sciences of Western Switzerland (HES-SO), 1400 Yverdon-les-Bains, Switzerland
[3] Department of Engineering Sciences, Uppsala University, Uppsala, Sweden

* Corresponding author. E-mail address: antonio.sunjerga@epfl.ch.

Abstract— Upward lightning occurs generally from tall structures. The mechanism of the initiation of upward lightning is not yet fully understood. Upward lightning can be classified into two categories based on either the absence or the presence of other lightning activity prior to the upward flash. This work proposes an explanation of how upward lightning flashes can be triggered by nearby lightning activity. It is generally thought that the lightning activity prior to the flash will intensify the electric field at the tip of the tall structures. However, to the best of our knowledge, no attempt has been made to evaluate theoretically this hypothesis. In this paper, we derive analytically the electric field enhancement on the ground (or at the top of tall structures) based on different triggering scenarios. These fields are later used in a simplified corona model to evaluate if they are able to trigger upward lightning. It is shown that both slow processes such as leader propagation and faster return strokes can trigger an upward negative flash from relatively short structures of a few tens of meters, even without any slowly varying background electric field. This study confirms theoretically experimental observations and it provides new insights into the mechanisms of initiation of upward flashes from tall structures.

Index Terms—: Lightning, upward, tall structure, other-triggered, analytical, nearby lightning, initiation, electrostatic, corona, sustained leader, criteria

1. Introduction

The characteristics of upward lightning discharges observed on tall towers (e.g., Gaisberg, Peissenberg, Säntis) have been widely reported in the literature (e.g., [Smorgonskiy et al. (2011)]). However, their initiation mechanisms are not well understood and are still under analysis.

Knowing the background thunderstorm electric field, the electric field at the tip of the tower can be estimated by electrostatic modeling. However, once the electric field reaches the critical breakdown value, corona discharges will be initiated reducing the electric field in the vicinity of the tower tip. In case of a positive corona discharge, the electric field will ionize the air and electrons will move toward the tower tip, while positive ions will drift in the electric field creating positive ion space charge near the tip of the tower, reducing the value of electric field. It is well known that a moving rocket in rocket-triggered lightning is more likely to initiate upward lightning at a given altitude than a tall structure of the same height as the altitude of the rocket [Uman (1987)], presumably because the corona charges are left behind the tip of the rocket.

Similarly, it has been hypothesized [Rachidi et al., 2008] and later confirmed by observations [Montanyà et al. (2014)] that a rotating wind turbine blade is more likely to initiate upward lightning compared to a still one. This is due to the fact that there is less time for the corona charge to build up as the object is moving and any corona charges that are generated are left behind by the moving blade tip.

The electric field distribution is governed by coupled electrostatic and charge balance equations. In order to have an upward leader initiated from the tip of a tower, the electric field has to exceed a critical value not only at the tip of the tower, but also along some critical distance [Cooray (2013)]. The electric potential of the tall structure has to be high enough for the initiated leader to be sustained and for it to escape from the corona charge cloud; otherwise, it will end up as what is known as an aborted leader [Wang et al. (2008)].

Based on a simplified model, Aleksandrov et al. (2001) derived analytical equations to determine the conditions for the development of an upward leader. The main input to their model is the induced voltage at the tip of the tower with respect to the ground, which is directly related to the background electric field and the height of the structure. The main conclusion of their work was that beyond a certain value of the background electric field for a given geometry, a sustained upward leader will be initiated. However, as shown in Aleksandrov et al. (2001), this value depends not only on the peak electric field, but also on its waveform. Electric field waveforms with fast risetimes are capable of initiating a sustained upward leader at lower values of the maximum electric field. Assuming a background electric field of 10 kV/m and a rise-time of about 10 s, the structure would need to be taller than 400 m to initiate a sustained upward leader. Based on their analysis, Aleksandrov et al. concluded that it is more likely that an upward leader be triggered by preceding nearby in-cloud or cloud-to-ground lightning activity than by the slow varying background electric field. Since in-cloud and cloud-to-ground flashes contain processes characterized by risetimes lower than few milliseconds, they would be able to initiate a sustained upward leader even from moderately tall structures with the same value of the electric field. This was first suggested by Berger and Vogelsanger (1969). It is worth noting that electric field changes caused by lightning are hypothesized to trigger discharges in the middle and upper atmosphere such as red sprites and elves (see Chapter 14 of Rakov and Uman, 2003).

Wang et al. (2008) proposed the classification of upward flashes into two categories: self-triggered (ST) and other-triggered (OT), based on either the absence or the presence of prior lightning activity in the geographical and temporal vicinity of the tower-initiated flash. The relative number of ST and OT flashes has been shown to vary depending on the geographical area (see e.g., [Smorgonskiy et al. (2015)]). For example, at the Gaisberg Tower [Smorgonskiy et al. (2015a)], only 13% of the flashes occur after prior lightning activity in the vicinity of the tower. On the other hand, in Rapid City [Warner et al. (2012)], observations from ten tall towers have shown that out of 81 upward flashes, only one was not preceded by other lightning activity, as determined by optical observations. The reported statistics on the percentage of triggered flashes could be underestimated since some of the preceding flashes could be missed depending on the type of data used for the classification [Sunjerga et al. (2018), Sunjerga et al. (2020a)].

It is worth noting that ST flashes have been observed at structures with much shorter height than those suggested by Aleksandrov et al. This might be due to the fact that the electric field can significantly exceed the value of 10 kV/m for some short period of time. Also, some of the structures are located on mountaintops, causing further enhancement of the field. The concept of effective height was introduced to account for the increased number of upward flashes from a tower located on a mountaintop [Rakov and Uman (2013), Smorgonskiy et al. (2012)].

OT flashes can be preceded (or triggered) by both in-cloud (IC) and cloud-to-ground (CG) flashes. Schumann et al. (2019), using video observations, proposed different mechanisms conducive to the initiation of upward flashes, all of them associated with horizontally propagating leaders in the clouds over the towers. It was assumed that the horizontal leaders produce an enhancement of the electric field at the tip of the tower, initiating an upward flash. To the best of our knowledge, no quantitative analysis has been performed to evaluate the field enhancement.

The aim of this paper is to estimate the salient parameters (such as peak value and risetime) of the electric field waveforms associated with the different nearby lightning triggering scenarios observed by Schumann et al. Furthermore, we investigate to which extent the estimated electric fields are able to initiate a sustained upward leader. The analysis is performed for an upward negative lightning and a positive corona discharge. A simplified, closed-form formula for the electric field at ground level as a function of time is derived that is applicable both, to the case of a horizontal and of a vertical leader. The ground is assumed to be a perfect electric conductor. To evaluate the criterion for the leader initiation, the electric field at ground level is then used as an input to the simplified, analytical corona discharge model for tall structures that was proposed by Aleksandrov et al. (2001).
The rest of the paper is organized as follows. Section 2 presents a brief description of the triggering scenarios proposed by Schumann et al. (2019). Section 3 presents simulations of the vertical electric field for each of these scenarios. In Section 4, we evaluate if these typical electric field changes can trigger an upward flash from a tower-like structure. Discussion is given in Section 5 and conclusions in Section 6.

2. Description of Scenarios

Saba et al. (2016) and Schumann et al. (2019) observed different scenarios leading to the triggering of an upward flash from a tower. All of them are characterized by a horizontal leader propagation over the tower. Some scenarios additionally include the presence of a vertical channel approaching the ground.

Figure 1 presents simplified sketches of the four scenarios observed to trigger upward negative lightning from the tip of the tower with the occurrence statistics. Schumann et al. (2019) reported occurrence statistics from both hemispheres at two observations sites in Rapid City and in Sao Paulo. Relatively similar occurrence statistics have been observed at these two sites (see Table 2 of Schumann et al. (2019)). The reported values in Figure 1 are average values taking in account sample sizes from these two sites.

In the first scenario (Figure 1-i), a bidirectional in-cloud leader is initiated near the tower and develops horizontally with its negative end approaching the tower while its positive end stretches away from the tower. Note that the positive leader part is shorter in length compared to the negative part since the positive leader speed has been observed to be smaller than the negative leader speed [van der Velde and Montanyà, 2013].

Upward lightning was also observed to occur prior to the attachment to ground of these leaders (Scenario 2), as shown in Figure 1-ii.

If the mechanisms described in scenarios 1 and 2 did not trigger an upward flash, this could happen after the connection of the downward leader to the ground and the initiation of the positive return stroke (RS), as illustrated in Figure 1-iii.

Finally, if none of the previous stages of the CG flash started as a horizontal in-cloud bidirectional leader trigger an upward flash, this could happen during the continuous current (CC) phase after the RS while the negative leader is extending in the direction of the tower as shown in Figure 1-iv.

Note that we assume that the positive RS neutralizes only the positive end of the leader while the negative one remains negatively charged. Once the downward leader reaches the ground Figure 1-iii the return stroke will neutralize the positive charges while the negative ones will be kept in place by cloud positive charges. Furthermore, if the charge from the negative cloud leader was also removed, since a bidirectional in-cloud leader is believed to have a zero-net charge, one would measure zero charge transfer in the channel-base current measurements which was not observed in measured downward positive flashes. If the negative charge were also to be neutralized by the positive RS, this would cause an electric field change at the tower opposite to the one leading to a negative upward flash, making the initiation of an upward leader according to the scenario 3 in Figure 1-iii even less likely. The removal of the positive charge of the leader could actually enable the negative part of the leader to spread even more freely and rapidly, as observed, at least for an opposite polarity flash in [Stock et al. (2017)].

The four scenarios illustrated in Figure 1 are arranged in a chronological order of occurrence. However, the scenarios in Figure 1-(i, ii and iv) share similar physical properties as they are all caused by relatively slow leader propagation. On the other hand, the scenario in Figure 1-iii is governed by the RS process that can be three orders of magnitude faster than leader processes.

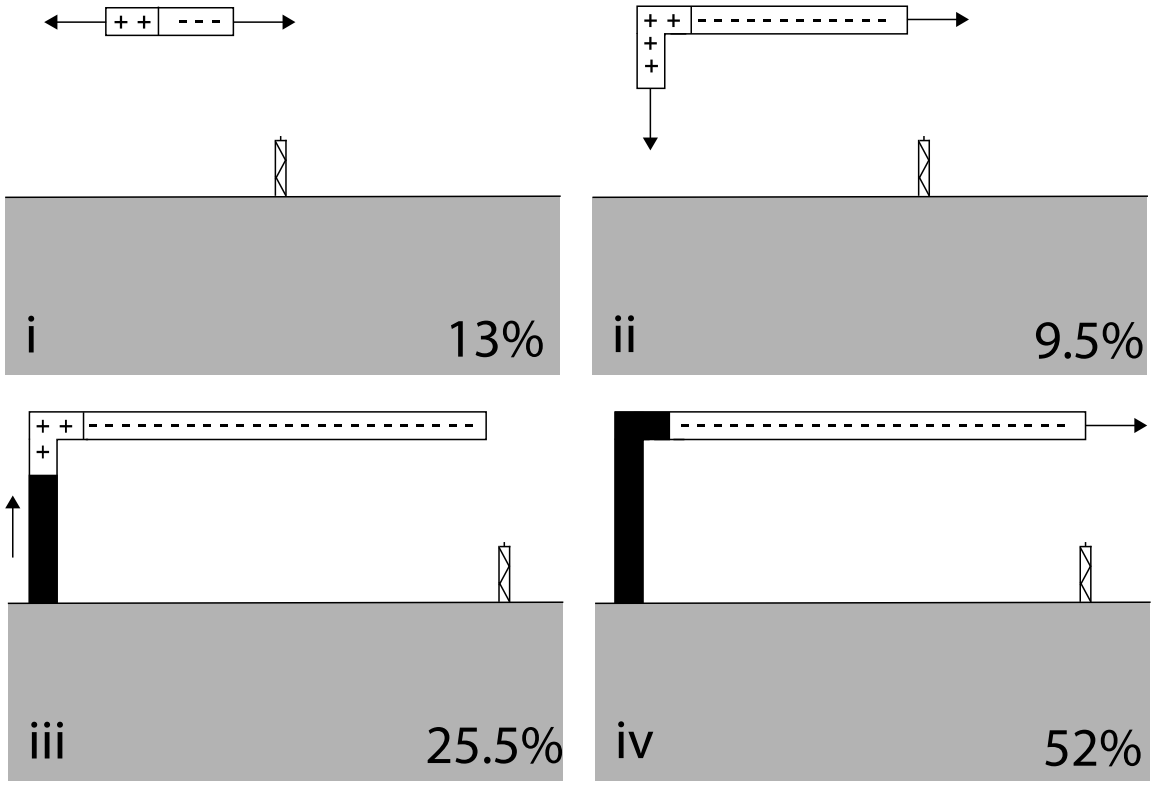

Figure 1. Typical scenarios leading to the triggering of a negative upward flash from a tower. (i) In-cloud leader above the tower, (ii) in-cloud leader prior to a positive RS, (iii) positive RS, (iv) CC extending the negative leader above the tower. Not to scale. The percentage of occurrence of these scenarios as observed by Schumann et al. (2019) is given in each panel.

3. Electric Field Characteristics of the Considered Scenarios for the Triggering Events

The aim of this section is to evaluate the electric fields caused by the considered triggering scenarios. We will consider possible ranges of the 10-90% risetime and peak (Figure 2) of the electric field by varying the geometrical properties, the velocity of propagation and the charge density of the leader.

Note that we are only considering scenarios for the initiation of an upward negative lightning (upward positive leader). Similar mechanisms have been observed in the case of an upward positive lightning (upward negative leader), in which an approaching positive leader leads to the initiation of an upward negative leader (for example, see Figure 14 in [Sunjerga et al. (2020a)]. In this section, we present the electric field expressions derived for each considered scenario. The full derivation can be found in the Appendix. Physics sign convention for the electric field was used in this paper (upward directed field is positive). It is worth noting that here we present a limited number of cases that are representative of common processes, having in mind uncertainties in input variables, including the input geometry, line charge density [e.g., Shen et al. 2019, Gao et al. 2020] and velocity of leaders [e.g., Proctor 1997, Campos et al. 2014]. An open-source code with a graphical interface is provided as supplementary material. Interested readers can use it to run any specific case.

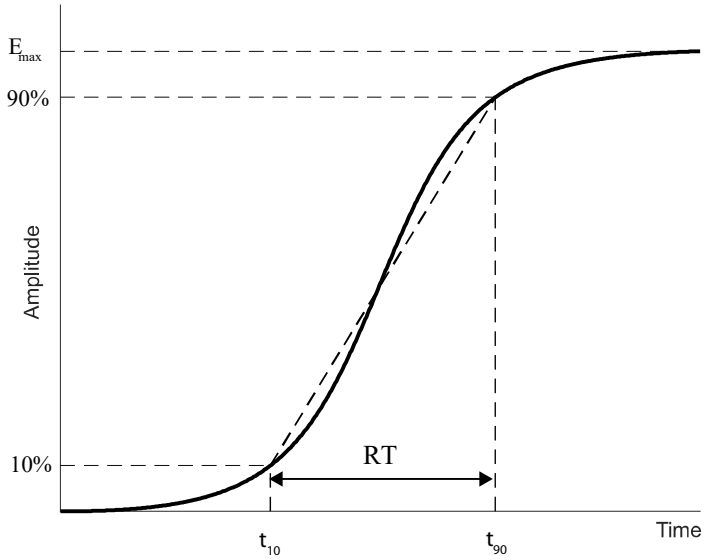

Figure 2. Definition of the electric field waveform parameters: 10-90% risetime (RT) and field peak.

3.1 Scenario 1: In-cloud leader

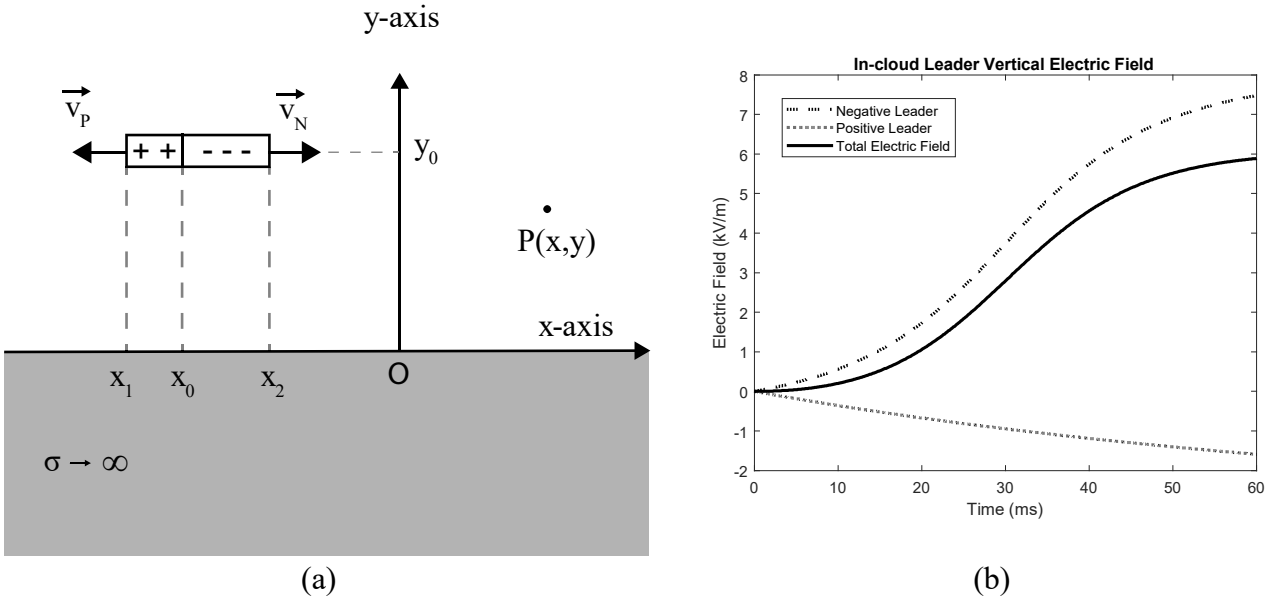

(a) (b)

Figure 3. In-cloud leader. (a) Geometry of problem. (b) Vertical electric field on the ground surface at the origin of the coordinate system. The computation parameters correspond to Case 2 of Table 1. The contributions of the negative and positive leaders are also presented. The origin of time (t=0) corresponds to the initiation of the bidirectional leader.

Figure 3a presents the geometry of the problem. The vertical electric field associated with this scenario at a given point P(x,y) is given by:

$$E_{y\,sc1}(x,y,t) = \frac{\lambda_N (y - y_0)}{4\pi\varepsilon_0}\left(f_{2H}(x,y,x_0,x_0 + v_N t, y_0) - \frac{v_N}{v_P} f_{2H}(x,y,x_0 - v_P t, x_0, y_0)\right) \quad (1)$$

where ε_0 is the vacuum permittivity, λ_N is the negative charge density, v_N and v_p are the propagation speeds of the negative and positive leader branches, and the function f_{2H} is defined in equations (A.9-A.13) in the Appendix.

Note that the adopted line charge density of the positive leader is such that the overall zero charge condition [Kasemir, 1960] along the whole bidirectional leader is satisfied.

The resulting electric field waveform will depend on many input parameters, of either geometrical or physical nature. For example, we can directly see from (1) that the electric field has a linear dependence on the charge density. On the other hand, the amplitude will also depend on the height of the leader above the ground as well as the starting point of the bidirectional leader ($x = x_0$ in Figure 3). The risetime will be governed by the velocities of the positive and negative leaders. Note that, in our model, we do not consider any branching of the channel.

We will analyze three different cases as described in Table 1. Case 2 corresponds to typical values expected from in-cloud bidirectional leaders at an altitude of 2 km above the ground [van der Velde and Montanyà, 2013]. Case 1 corresponds to a low charge density leader characterized by the smallest expected propagation velocities and initiated at a height of 4 km above the ground. Case 3 corresponds to the highest expected line charge density and propagation velocities for a leader located only 1 km above the ground. The charge density obtained for this maximum charge density case (1.5 C/km) is similar to the values observed by Proctor (1997) from measurements of stepped leaders. The charge density values for the other cases are similar to those obtained by Shen et al. (2018).

Figure 3b presents the contributions of the positive and the negative leaders to the total electric field at the origin of the coordinate system for Case 2. At early times, the contributions of the positive and negative leaders are similar in magnitude because of their similar relative distance to the observation point (origin of coordinate system). However, as the negative leader progresses to the right and approaches the origin, it becomes dominant.

A comparison of the electric field waveforms associated with the three different cases is shown in Figure 4a. Differences in both peak amplitude and waveshape can be observed. Figure 4b presents the 2-D distribution of the vertical electric field for Case 2, 60 ms after the initiation.

Table 1. Input parameters and the resulting rise time (τ) and peak electric field (E_{max}) for Scenario 1: In-cloud leader

	λ_N[C/km]	H [km]	v_P [m/s]	v_N [m/s]	x_0 [km]	RT[ms]	E_{max}[kV/m]
Case 1	-0.1	4	$1x10^4$	$5x10^4$	-1.5	39	0.06
Case 2	-0.5	2	$2x10^4$	$1x10^5$	-3	31	5.8
Case 3	-1.5	1	$4x10^4$	$2x10^5$	-6	12	52

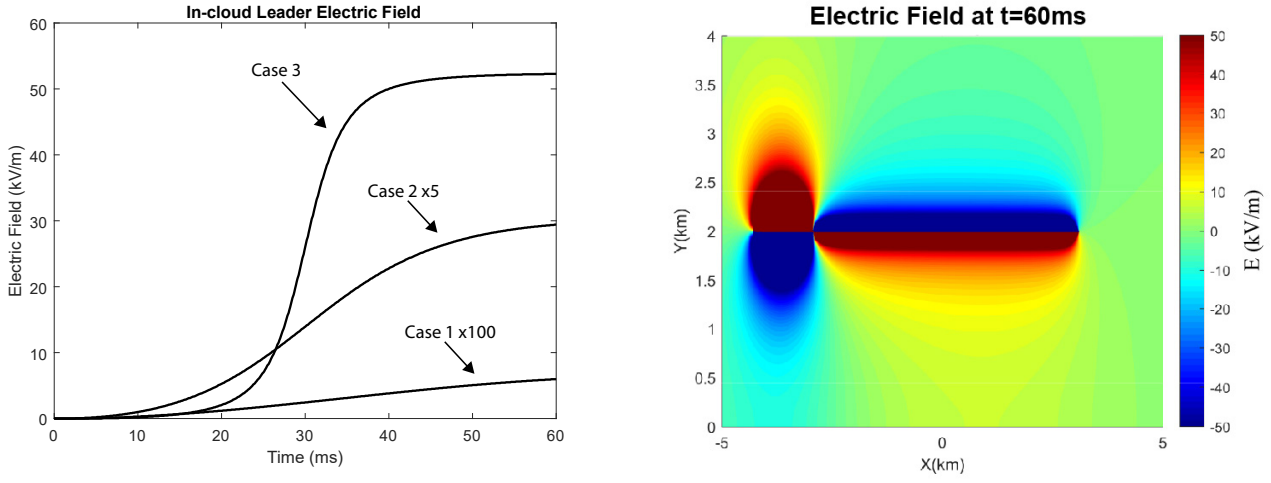

(a) (b)

Figure 4. Scenario 1: (a) Vertical electric field waveforms at the origin of the coordinate system for the three considered cases. (b) 2D distribution of the vertical electric field for Case 2 at 60 ms.

3.2 Scenario 2: Positive leader approaching the ground

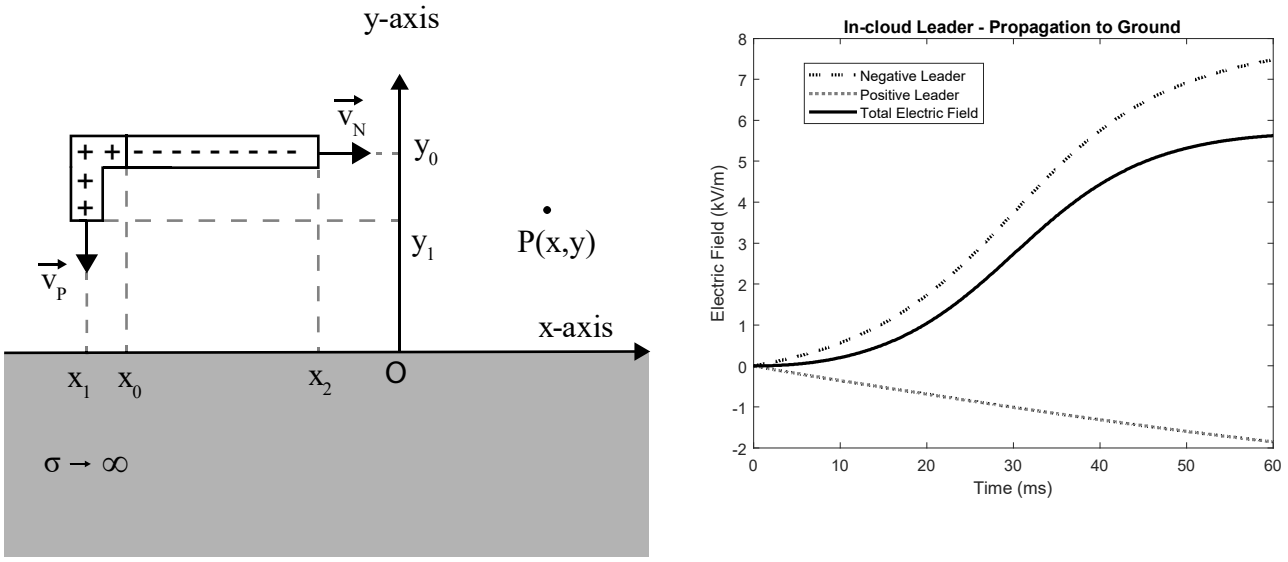

(a) (b)

Figure 5. Scenario 2: In-cloud leader propagation to ground. (a) Geometry of problem. (b) Components of the vertical electric field at the origin of the coordinate system for Case 2a. The origin of time (t=0) corresponds to the initiation of the bidirectional leader.

Figure 5a presents the geometry of the scenario. The vertical electric field at a given point P(x,y) is given by:

$$E_{y\,sc2}(x,y,t) = \begin{cases} E_{y\,sc1}(t), & t \le T_1 \\ E_{y2}(t), & t > T_1 \end{cases} \tag{2}$$

where T_1 is the moment in time when the positive leader starts to propagate toward the ground, and $E_{ysc1}(t)$ is the field associated with Scenario 1 given by (1). E_{y2} is given by

$$E_{y2}(x,y,t) = \frac{\lambda_N (y-y_0)}{4\pi\varepsilon_0}\left(f_{2H}(x,y,x_0,x_0+v_N t,y_0) - \frac{v_N}{v_P} f_{2H}(x,y,x_0-v_P,T_1,x_0,y_0)\right) - \frac{\lambda_N v_N}{4\pi\varepsilon_0 v_P} f_{2V}(x,y,x_{T_1},y_0 - v_P(t-T_1) \tag{3}$$

The functions f_{2H} and f_{2V} are defined in the equations (A.9-A.13) and (A.24-A.28) in the Appendix. Note that the line charge density of the positive leader is such that the overall zero charge condition along the whole leader is satisfied.

Three different cases are considered whose parameters are presented in Table 2. These cases are similar to Case 2 in Scenario 1 (in terms of leader charge density, propagation speeds, height) with the difference that, here, we vary the location along the x-axis of the initiation of the bidirectional leader and the time T_1 after which the positive leader veers towards the ground. It is also worth mentioning that the velocity of a downward stepped leader increases as it approaches the ground [Campos et al. (2010)]. However, for the sake of simplicity, we consider it to be constant in this study.

As can be seen from the results presented in Figure 5b, the vertical positive leader will result in a smaller overall peak electric field compared to Scenario 1. As expected, it can be seen on Fig- 6a that the closer the positive leader to the observation point, the higher the decrease in the field. If the leader gets sufficiently close to the observation point, the electric field could even change sign and become negative. Figure 6b presents the 2D distribution of the vertical electric field for Case 2a, 60 ms from the initiation of the leader.

Table 2. Input parameters and the resulting rise time (RT) and peak electric field (E_{max}) for Scenario 2: In-cloud leader propagation to the ground. For λ_N=-0.5 C/km, H=2 km, v_P=2x10^4 m/s, v_N=1x10^5 m/s and T_1=10 ms			
	x_0 [km]	RT [ms]	E_{max}[kV/m]
Case 2a	-3	31	5.75
Case 2b	-2	22	3.5
Case 2c	-1	18	1

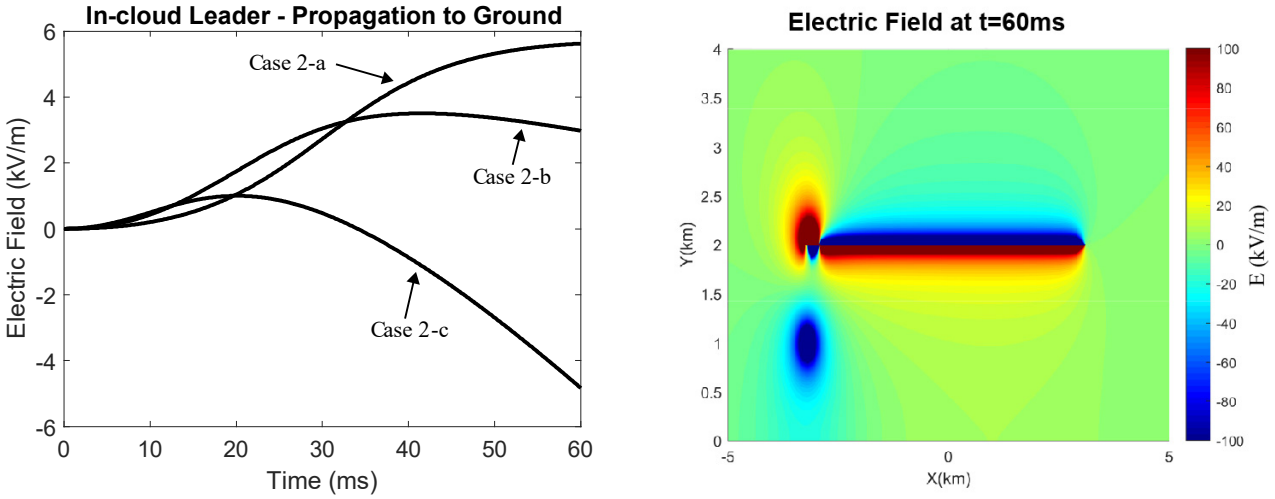

(a) (b)

Figure 6. (a) Electric field waveforms at the origin of the coordinate system for the three considered cases (Table 2) in Scenario 2. (b) 2D distribution of the vertical electric field for Case 2a at 60 ms.

3.3 Scenario 3: Positive return stroke

Positive flashes are less common than negative flashes. Their current waveform is typically characterized by slower risetimes and it can have an order of magnitude higher peak value compared to negative flashes [Rakov (2013)]. Cooray (1995 and 2000) was the first to develop a model for positive return strokes. For the sake of simplicity and considering the relatively small distance to the observation point, we will consider here only the electrostatic field of the return stroke. At distances not exceeding a few kilometers, the late-time electric field is mostly due to the electrostatic field component in case of negative return strokes as discussed by Lin et al. (1979). We assume here that the electrostatic assumption would hold for a positive return strokes due to its slower risetime.

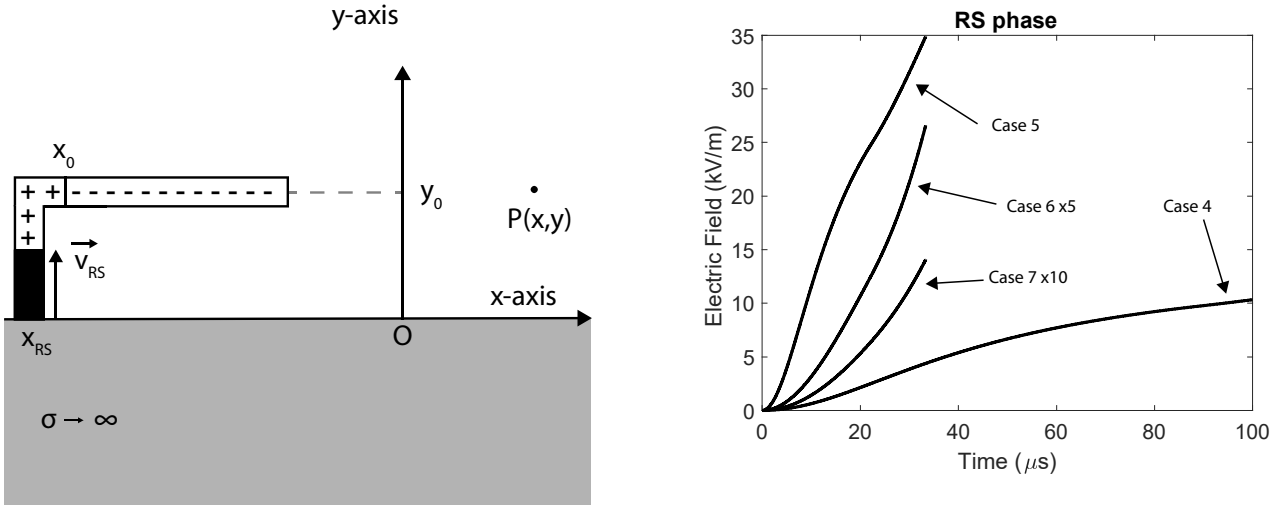

(a) (b)

Figure 7. Scenario 3: Positive RS (a) Geometry of the problem. (b) Vertical electric field at the origin of the coordinate system for the considered cases in Table 4. The origin of time (t=0) corresponds to the initiation of the return stroke.

Figure 7a presents the geometry of the problem. The vertical electric field at a given point P(x,y) is given by:

$$E_{y\,sc3}(x,y,t) = \begin{cases} E_{y1}(t), & t \le T_2 \\ E_{y2}(t) = E_{y1}(T_2) + E_{y2}(t), & t > T_2 \end{cases} \quad (4)$$

where T_2 is the moment in time when the return stroke reaches the maximum altitude y_0 and starts to propagate in the horizontal direction. E_{y1} and E_{y2} are given by

$$E_{y1}(x,y,t) = -\frac{\lambda_P}{4\pi\varepsilon_0} f_{2V}(x,y,x_{RS},0,v_{RS}t) \quad (5)$$

$$E_{y2}(x,y,t) = -\frac{\lambda_P}{4\pi\varepsilon_0}\left(f_{2V}(x,y,x_{RS},0,v_{RS}T_2) + (y-y_0) f_{2H}(x,y,x_{RS},x_{RS}+v_{RS}(t-T_2),y_0)\right) \quad (6)$$

in which the geometrical functions f_{2H} and f_{2V} are defined in equations (A.9-A.13) and (A.24-A.28) in the Appendix.

We will consider three different distances from the vertical leader, as specified in Table 3. The assumed charge density is 2.5 C/km [Thomson et al. 1985]. The assumed return stroke speed is $0.9\text{x}10^8$ m/s, which corresponds to typical observed speeds [Cooray (2000)]. We consider two different heights for the return stroke (or altitudes for the horizontal leader). The lower one could be associated with positive flashes caused by the lower positive charge pocket, and the higher to flashes caused by the upper main positive charge region [Rakov (2013)]. Note that, in Table 3, E_{max1} is the field observed at the origin at the moment when the return stroke reaches the point (x_{RS},y_0), while E_{max2} is the field at the moment when the return stroke reaches the initiation point of the bidirectional leader (x_0,y_0).

The magnitude of the electric field will mostly depend on the distance to the observation point. The observed risetimes are much smaller compared to risetimes associated with leader fields, since the return stroke speed is much faster than the leader propagation speed.

Table 3. Input parameters and the resulting rise times (RT) and electric fields (E_{max1} and E_{max2}) for Scenario 3: positive RS. For λ_P=2.5 C/km and v_{RS}= $0.9\text{x}10^8$ m/s

	H [km]	x_{RS} [km]	x_0 [km]	RT [μs]	E_{max1}[kV/m]	E_{max2}[kV/m]
Case 4	8	-3	-2	68.2	9.7	10.3
Case 5	2	-1	0	25.2	24.8	34.9
Case 6	2	-3	-2	22.6	2.5	5.32
Case 7	2	-5	-4	21.7	0.64	1.4

Figure 8 presents the spatial distribution of the vertical electric field at the time instant when the whole positive leader is neutralized for cases 4 and 5 in Table 3. As expected, the maximum value of the electric field occurs at the base of the vertical leader since the contribution of the channel elements and their images add-up constructively to yield a maximum value.

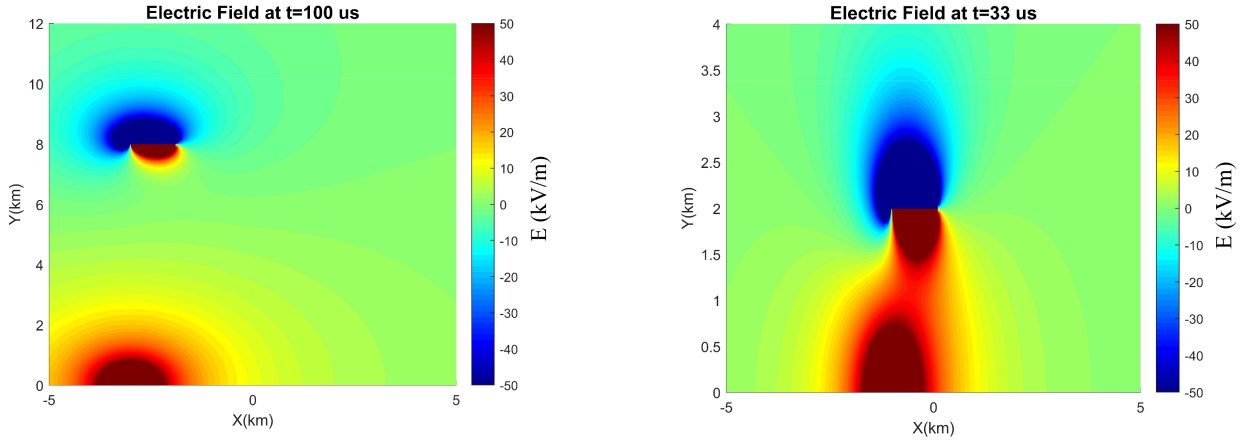

(a) (b)

Figure 8. 2D distribution of the vertical electric field at the time instant when the whole positive leader is neutralized. (a) Case 4. (b) Case 5.

3.4 Scenario 4: Developing horizontal leader during the continuous current phase

Figure 9a presents a sketch of Scenario 4, according to which a horizontal leader develops above the tower during the CC phase following a positive return stroke. Note that the positive part of the leader is already neutralized by the return stroke preceding the CC phase. We evaluate here the electric field change caused by the extension of the negative leader from its location right after the RS.

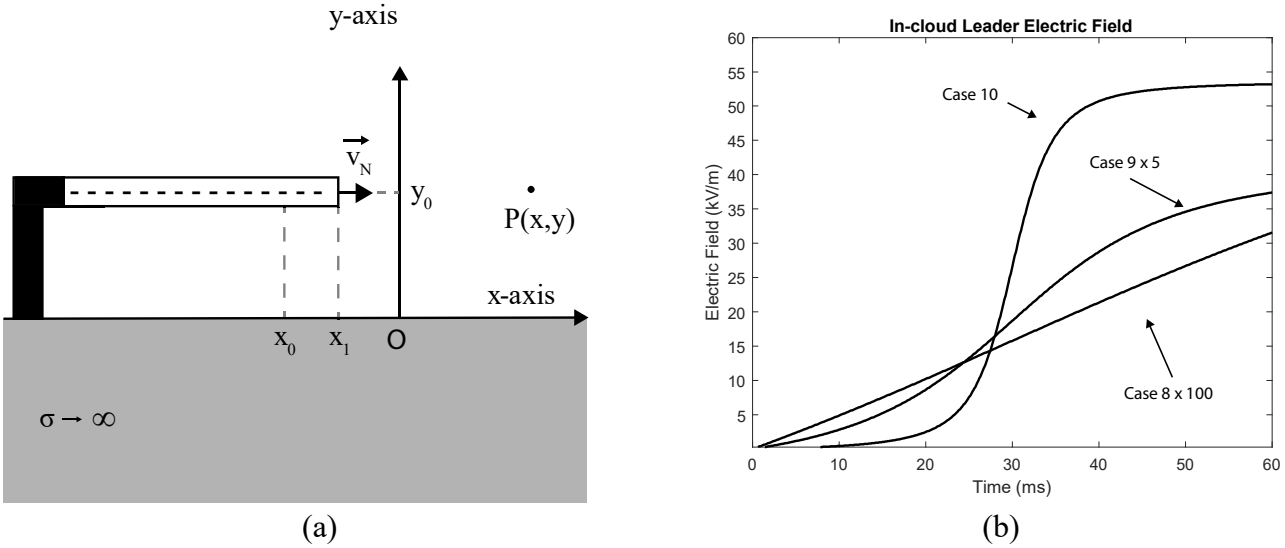

(a) (b)

Figure 9. Scenario 4: Horizontal leader during the continuous current phase following a positive return stroke. (a) Geometry of problem. (b) Vertical electric field at the origin of the coordinate system for the three considered cases (cases 7, 8, and 9). The origin of time (t=0) corresponds to the start of the horizontal leader extension during the continuous current phase.

With reference to Figure 9a, the vertical electric field a given point P(x,y) is given by:

$$E_{y\,sc1}(x,y,t) = \frac{\lambda_N(y-y_0)}{4\pi\varepsilon_0}\, f_{2H}(x,y,x_0,x_0+v_N t,y_0) \tag{7}$$

where the geometrical function f_{2H} is given in equations A.9-A.13 in the Appendix.

The resulting electric fields are calculated for three different cases with the same leader parameters (see Table 4) as in Scenario 1 (In-cloud leader). The resulting waveforms are somewhat similar to the ones

obtained in Scenario 1 (In-cloud leader) with higher peaks in Scenario 4 because the absence of the positive end of the leader increases the value of the field. This latter reason is particularly evident in Case 1 (Case 8 in Scenario 4), where the leader is at a high altitude above the ground and the contribution of the positive leader is close to the one of the negative leader, as their distances to the observation point are similar. The risetimes observed in Scenario 4 are similar to those in Scenario 1 (In-cloud leader) since they are mostly governed by the velocity of the negative leader.

Table 4. Input parameters and the resulting rise time (RT) and peak electric field (E_{max}) for Scenario 4: Horizontal leader during the CC phase

	λ_N[C/km]	H [km]	v_N [m/s]	x_0 [km]	RT [ms]	E_{max}[kV/m]
Case 8	-0.1	4	$5x10^4$	-1.5	46.8	0.32
Case 9	-0.5	2	$1x10^5$	-3	35.6	7.47
Case 10	-1.5	1	$2x10^5$	-6	12.8	53.2

4. Upward Lightning Initiation Criteria

4.1 Aleksandrov et al. model for the corona discharge

This section is based on the simplified analytical model developed by Aleksandrov et al. (2001) where the corona discharge from the tip of a tall structure (Figure 10a) is represented by a spherical electrode in free space as shown in Figure 10b (r_1, which tends to infinity, denotes the distance to the reference for the potential difference calculation), imposing the condition that the total potential on the surface of the sphere is at the same potential as the ground. This model neglects the contribution of the charges along the structure. Assuming a constant electric field along the z-axis, the background potential at the location of the sphere at the altitude h is $-Eh$, so that, in order to satisfy zero total potential condition, the potential due to the charge on the sphere is given by:

$$U \approx E_y h, \qquad (8)$$

Now, assuming that the background electric field is not significant near the sphere compared to the electric field due to the charge on the sphere, this simple corona model can be used, as a first approximation, to evaluate the electric field on the top of a tall structure in the presence of corona charges. A more rigorous approach would require discretizing the structure and its image into elementary parts and imposing the zero-potential condition on each element. This procedure is used in the charge simulation method developed by Singer et al. (1974). That approach, although more accurate, is not used here because it does not allow a fully analytical solution. Aleksandrov et al. (2002) estimated the accuracy of the simplified sphere model by comparing it to a more realistic model of a grounded rod of height h and a hemispherical top of the same radius as the sphere, and they observed that the simple sphere model overestimates the electric field by a factor of less than two.
This simplified model is good enough for the analysis of the field near the electrode and it can yield more insights into the upward triggering mechanism using a qualitative analysis. If one were interested in obtaining the electric field at ground level next to the structure, the elaboration of a more realistic model of the structure would be needed. Such analysis was done analytically by Smorgonskiy et al. (2015b) and numerically by Arcanjo et al. (2018), both based on the charge simulation method. Observations show that, depending on the height of the object, the measured electric field could be more than ten times lower than the background electric field.

Note that, in our analysis, the background electric field will be caused either by the leader or by the return stroke, depending on the particular scenario being considered (see Figure 1). Here, we will briefly summarize the approach presented by Aleksandrov et al. (2001). The interested reader is referred to the original paper for more details.

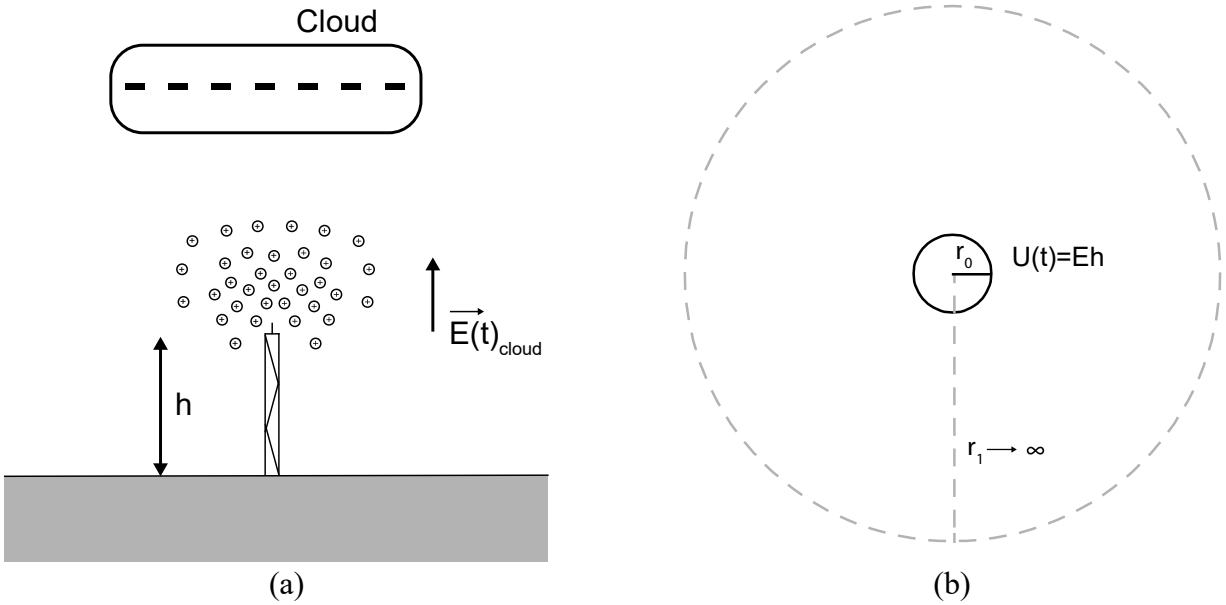

Figure 10. Corona discharge from the tip of a tall structure. (a) Positive corona discharge at the tip of a tall structure in the electric field of the cloud (adapted from Aleksandrov et al. (2001)). (b) Simplified model representing the corona discharge using a spherical electrode in free space.

If the electric field on the surface of the sphere is lower than the critical breakdown electric field, then the electric potential at a distance r from the center of the sphere in space outside of the sphere is obtained by solving Poisson's equation and the solution is:

$$U_{no\ corona}(r) = \frac{Ehr_0}{r} \tag{9}$$

As soon as the field on the surface of the sphere exceeds the breakdown electric field (around 3 MV/m under standard conditions for an electrode with a radius bigger than a few centimeters), streamer-free corona discharge (electron avalanche), and therefore a current will be initiated. In order to evaluate the electric field, one has to solve the electrostatic Poisson's equation coupled with the balance equation for the space charge. Aleksandrov et al. (2001) obtained the following solution for the electric field as a function of the radial distance r outside of the sphere:

$$E(r) = \frac{1}{r^2}\sqrt{E_C^2 r_0^4 + \frac{i(t)(r^3 - r_0^3)}{6\pi\varepsilon_0\mu}} \tag{10}$$

where μ is permeability of the vacuum, E_C is the threshold corona field and $i(t)$ is the current that can be obtained for the case of a voltage applied to the sphere as a result of the background electric field, of the form $U=U_m t^k$ at $t \leq \tau_A$ and $U=U_m$ at $t > \tau_A$ as:

$$i(t) = 2\pi\varepsilon_0 U^{\frac{3}{2}}(t)\sqrt{\frac{(k+1)\mu}{6t}} \tag{11}$$

the radius of the expanding ion cloud is given by:

$$R(t) = \sqrt{\frac{2\mu U(t)t}{3(k+1)}} \tag{12}$$

in which $\mu=1.5\ cm^2V^{-1}s^{-1}$ is the ion mobility [Chauzy & Rennela, 1985], r_0 is the radius of the sphere, and U is the voltage between the sphere and infinity (see Figure 10b) with peak value of U_m.
Figure 11a presents the electric field as a function of the radial distance considering two different risetimes for U. The voltage U is assumed to be linearly rising (k=1) up to the maximum voltage U_m= 2 MV, beyond which it stays constant. The radius of the sphere is r_0=5 cm. This voltage could be for

example induced on a 200-m tall structure under a background electric field of 10 kV/m (see equation 8). We can observe from Figure 11a that the electric field is reduced significantly by the influence of the corona charges, both in the case of slow (10-s risetime) and fast (30-ms risetime) changes. In both cases, the predicted field without taking into account the effect of the corona charge is equal to 40 MV/m at $r=r_0$ (not seen in Figure 11a since it is out of the scale). When the corona charge is taken into account, the electric field on the surface of the sphere is equal to 3 MV/m in both cases. The analysis also shows that the reduction of the electric field is about four times more significant at a distance of r = 0.5 m for the case of a slow process (10-s risetime) compared with a faster process (30-ms risetime). At farther distances, the predicted electric field disregarding the corona charges will become smaller than those taking into account corona, since most of the voltage drop occurs close to the sphere.

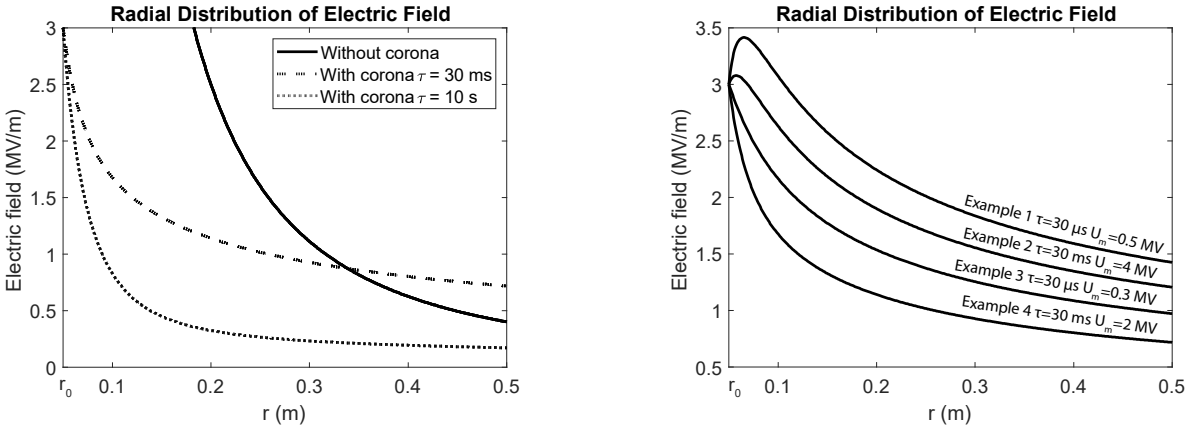

(a) (b)

Figure 11. Electric field at the time of maximum voltage as a function of the radial distance. (a) 10-s risetime and 30-ms risetime U_m=2 MV, r_0 = 5 cm. (b) 30-ms and 30-μs risetime for different peak voltages

4.2 Criteria for the Initiation of a Sustained Leader

In order for the streamers to be initiated from streamer-free corona discharge, the electric field has to be higher than the breakdown level over some critical length in front of the electrode. Note that corona discharge consists of both electron avalanches and streamers while Aleksandrov et al. (2001) refers to electron avalanche without streamers as streamer-free corona (see Figure 12). Aleksandrov et al. (2001) assumed that the condition

$$\left.\frac{\partial E(r,t)}{\partial r}\right|_{r=r_0} > 0 \qquad (13)$$

is sufficient for the streamers to be initiated.

Figure 11b presents four examples with different voltage risetimes and peaks. The two considered risetimes are characteristic of the cases analyzed in the previous section, namely the leader propagation and the return stroke. Example 1 and Example 2 satisfy condition (13). Note that, for low risetimes, which are characteristic of return strokes, much lower voltages are required to satisfy condition (13) than in a case of the longer risetimes associated with leader propagation (see Figure 13 below for more details).

In this section, we will discuss different criteria that have to be satisfied in order to have a sustained leader development. Once the electric field on the surface of the electrode reaches the critical breakdown electric field, streamer-free corona discharge will be initiated. This could lead to streamer initiation which is a necessary condition for the leader generation.

Further, if specific conditions are met, a leader will be initiated and, depending on the conditions, it can end up either as an aborted leader or continue to develop as a sustained leader. A graphical representation illustrating the necessary conditions leading to the leader initiation and development is shown in Figure 12, which refers to equations that are given below.

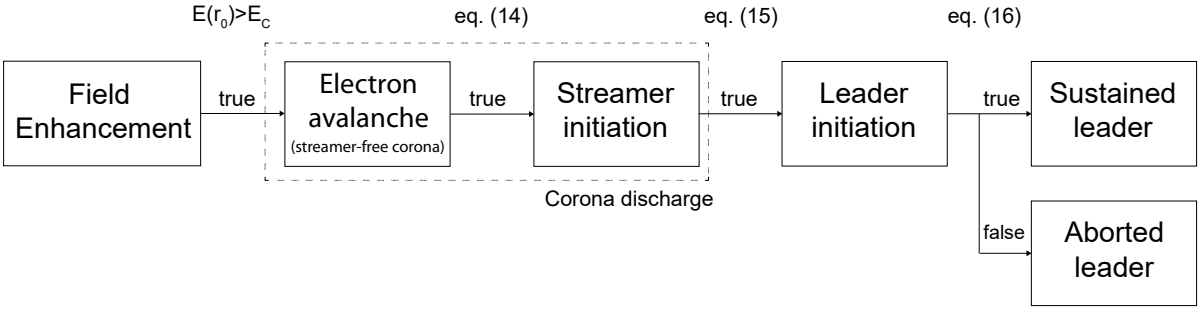

Figure 12. Conditions for sustained upward leader initiation.

In what follows, we will provide criteria for a sustained upward positive leader development as obtained by Aleksandrov et al. (2001). First, the electric field has to be higher than the critical breakdown electric field for the start of the streamer-free corona discharge.

Further, inserting (10) into (13), one can obtain a criterion for corona discharge (streamer-free) to streamer initiation for the case of a linearly rising voltage as:

$$U_m \geq 2E_C r_0 \left(\frac{6\mu E_C \tau}{r_0}\right)^{\frac{1}{3}} \qquad (14)$$

where τ is the risetime of the voltage and E_C is the critical electric field for the streamer-free corona discharge initiation.

Based on the fact that the minimum necessary length of the streamer zone for that streamer to evolve into leader called critical length (d_{cr}) is about 1 m [Meek and Craggs (1978), Bazelyan and Raizer (1998), Gallimberti (1979)], and that the voltage drop (ΔU_{min}) along that distance has to be at least 400 kV [Bazelyan and Raizer (1998), Bazelyan and Raizer (2000)], Aleksandrov et al. (2001) derived the following condition for the upward leader initiation:

$$U_m \geq \frac{3}{2}\left(\frac{\Delta U_{min}^4 \mu}{2d_{cr}^2}\right)^{\frac{1}{3}} \approx 1.86\,\tau^{\frac{1}{3}}\,[MV] \qquad (15)$$

This condition can be satisfied by a voltage with either sufficiently high magnitude or a sufficiently low risetime.

Furthermore, Aleksandrov et al. (2001) derived a criterion that has to be satisfied by an upward leader to escape the space charge cloud and not end up as aborted leader. This criterion is derived based on the condition that the background electric field is higher than the channel electric field opposing the former, so that the potential of the tip remains always higher than the background electric field potential. The criterion reads

$$U_m \geq 3.54\,\tau^{\frac{5}{16}}\,[MV] \qquad (16)$$

If (16) is not satisfied, the leader will stop propagating once the potential of the leader tip becomes equal to U_m. Note that (14-16) are derived for the case of a linearly rising voltage. In the following analysis, we use E_c=3 MV/m.

4.3 Criteria Evaluation

In this section, we will use the initiation criteria (inequalities (14), (15) and (16)) to assess the ability of the scenarios discussed in Section 3 to initiate upward lightning from a tall structure. We will only discuss the field changes caused by these processes and we will not take into account the background electric field, which usually has much slower risetimes in the order of several seconds. This assumption is supported by the fact that corona charges at the tall structure will have had enough time to neutralize the slow background field in the proximity of the tower.

In our model, Scenario 2 (Positive leader approaching the ground) is taking into account the field change due to the prior Scenario 1 process. In Scenario 3 (Positive RS), the influence of the prior two scenarios (1 and 2) is omitted since the risetime of the positive RS is three orders of magnitude lower than that of the prior processes. Moreover, in the case of Scenario 3, the leader in these prior scenarios does not necessarily have to be passing above the tower as shown in Figure 1-iii, they could be directed away from the structure of interest. Finally, in Scenario 4, prior processes are again omitted since we assume that if the RS was close to the tall structure, it would have already triggered an upward flash before the CC phase.

These assumptions are made in order to use the derived analytical solution to assess each scenario individually. For a more thorough analysis, numerical methods can be used to estimate the background electric field resulting from the different prior processes. Note finally that the contribution from the background electric field could either support or oppose the triggering of the upward flash. It is not unconceivable that for some cases in scenarios 3 and 4 that do not generate the required conditions to initiate an upward flash, the field contribution from prior processes could add constructively to support the initiation of an upward flash.

Criteria (15) and (16) only depend on the risetime and, for the risetimes of interest, the voltage given by criterion (16) is always higher that that given by (15). On the other hand (14) depends also on the radius of the sphere.

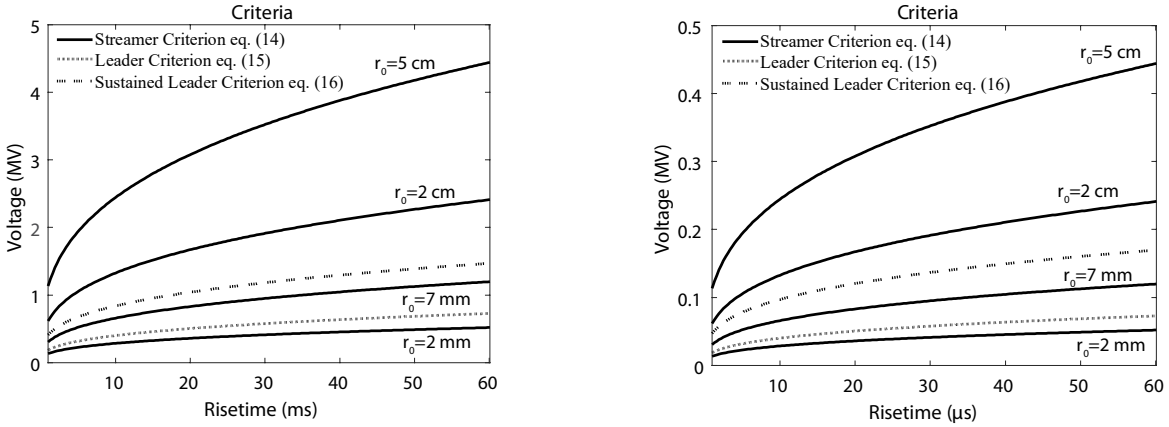

(a) (b)

Figure 13. Minimum voltage criteria for upward leader development from a tall structure as a function of the field risetime. (a) Risetime characteristic of leader processes. (b) Risetime characteristic of return stroke processes.

The criteria for the minimum voltage for each of the processes (streamer, leader, sustained leader) are shown in Figure 13 as a function of the risetime. For the streamer criterion, the results are shown considering four different radiuses for the equivalent spherical electrode. If we consider the radius of the sphere to be in the range of about 3 to 10 mm, all of the streamers will develop at least to aborted leaders. If the radius is less than about 3 mm, the leader initiation will require a higher field than that required for the streamer. It is worth also noting that for sphere radiuses of less than 1 cm, a higher error in the analytical model is expected as discussed in Aleksandrov et al. (2001).

Considering that the lightning rods are sharp, it is reasonable to assume that the sphere radius is less than 1 cm. According to the above analysis, for a sphere radius less than 1 cm, condition (16) for the sustained upward leader requires higher fields than those required for streamer and leader initiation. Table 5 presents for all the considered cases, the minimum height of the structure so that condition (16) for a sustained leader is satisfied.

In order to obtain the excitation voltage given as:

$$U(t) = \begin{cases} U_m t, & t \leq \tau \\ U_m, & t > \tau \end{cases} \tag{17}$$

from the simulated results in Section 3, we made the following assumptions. The simulated waveforms are linear in the range from t_{10} to t_{90} (see Figure 2). We assume that E_m is equal to the electric field difference from t_{10} to t_{90} or 80% of E_{max} (see Figure 2). The risetime τ is equal to RT ($t_{90} - t_{10}$). Further, we assume that the vertical electric field is constant along the height of the object so that U_m is simply given as the product of E_m with the height h. The resulting minimum heights of the structure to initiate a sustained upward leader are presented in Table 6 for the various considered cases.

Table 6. Minimum height of the structure for the initiation of a sustained upward leader

Case	E_m [kV/m]	τ	H [m]
1	0.06	39 ms	26759
2	5.8	31 ms	254
3	52	12 ms	21
2a	5.75	31 ms	260
2b	3.5	22 ms	384
2c	1	18 ms	1260
4	10.3	68 μs	21.4
5	35	25 μs	4.6
6	5.3	23 μs	29.4
7	1.4	22 μs	110
8	0.21	47 ms	5312
9	5	36 ms	209
10	50.1	13 ms	21

We can observe that a weakly charged leader as those analyzed in cases 1 and 8 are not likely to trigger a sustained upward lightning during the leader propagation phase. In Case 2c, a sustained leader is unlikely because of the decrease of the field due to the presence of a positive leader close to the observation point. All other cases shown can trigger an upward flash from a tower with a reasonable height. Strongly charged leaders such as those in cases 3 and 10 are also very likely to trigger a sustained upward leader. Also, all the cases 4-7 with a fast risetime corresponding to the return stroke phase are capable of triggering lightning from relatively low structures. Note that, for some cases, the assumption of a constant electric field along the structure is questionable because of the high value of the minimum height (cases 1, 2c and 8). However, these high values suggest that no upward flashes can be initiated under such conditions.

Figure 14 presents the critical value of the electric field change as a function of the risetime for structures of different heights. These heights are representative of modern wind turbines. We assume that the lightning rod is sharp enough so that the criterium in Eq. (16) is the most rigid one. Fast changes of about 1 kV/m typical for the nearby return strokes (distances of few km) can initiate a sustained leader while, in the case of slow risetimes typical of the nearby leader propagation, the electric field has to be several

times higher. Note that these values could be significantly lower if the background cloud charge electric field was also considered. Also, it is worth noting that the simplified sphere model overestimates (by a factor of about 2) the fields in the vicinity of the sphere. As a result, the critical electric field to initiate an upward flash might be higher.

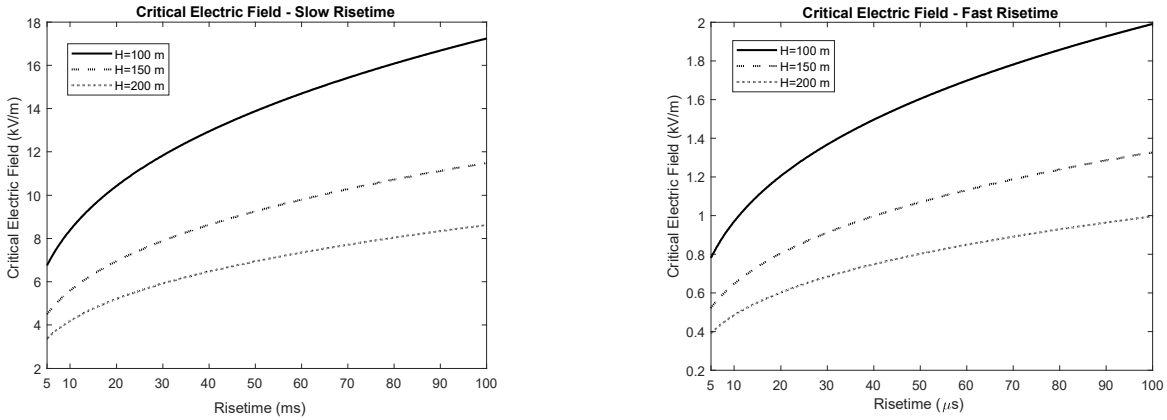

(a) (b)

Figure 14. Critical electric field change for development of sustained leader as a function of the risetime for different tall structure heights. (a) Risetime characteristic of leader processes. (b) Risetime characteristic of return stroke processes.

5. Discussion

A discussion is in order on the statistical occurrence of the observed scenarios, as reported by Schumann et al. (2019). For example, the lowest occurrence (9.5%) was observed for Scenario 2 (Positive leader approaching the ground), for which we observed the lowest magnitudes of the electric field. The fact that Scenario 4 (CC phase) has a much higher occurrence (52%) than Scenario 1 (In-cloud leader) with 13% can be explained by the higher amplitude of electric field and processes occurring prior to Scenario 4 (CC phase). Scenario 4 (CC phase) is preceded by scenarios 2 (Positive leader approaching the ground) and 3 (Positive RS), the contributions of which add up to the field enhancement at the tower. On the other hand, the relatively high occurrence of upward flashes after the RS phase might be due to its fast risetime and also to Scenario 2 (Positive leader approaching the ground) preceding it. Cloud-to-cloud lightning is about 2 to 10 times [Soriano and de Pablo (2007)] more common than cloud-to-ground lightning and this could explain the occurrence ratio of scenarios 1 (In-cloud leader) and 2 (Positive leader approaching the ground). For a more detailed analysis, one would have to take into account the general occurrence statistics of each scenario as well as the spatial extent. For example, while the RS is occurring at a given location, leaders can extend to several tens of km. We will not pursue this analysis since it is beyond the scope of this paper.

The obtained results presented in Figure 14a suggest that electric fields in the order of only 1 kV/m from return strokes of positive flashes can potentially initiate an upward flash from a 100-m tall structure. Such field intensities are typical of return strokes at distances as far as a few kilometers. This finding is supported by experimental observations. Warner et al. (2012) observed upward lightning flashes to 10 communication towers with heights ranging from 91 to 191 m, which were preceded by positive CG flashes that occurred at distances ranging from 3.5 to 49 km from the towers. Smorgonskiy et al. (2015a) reported upward flashes to the 100-m tall Gaisberg Tower preceded by positive CG lightning at distances ranging from 300 m to 48.3 km from the tower. The observed cases involving preceding CG flashes at longer distances (of some tens of km) could be due to different reasons such as

- the presence of a strong background electric field,
- errors in the estimates of the locations of the preceding CG flashes provided by lightning location systems,
- some of these distant preceding events might have happened by chance without any causality relation to the upward flashes [Rubinstein et al., 2016],
- the fact that negative leaders during the CC phase can propagate several tens of kilometers. The propagation of the negative leader along the cloud base during tens (sometimes hundreds) of milliseconds were frequently observed by high-speed cameras and/or lightning mapping arrays (LMA) for most of the cases analyzed in Brazil and the US (Saba et al., 2016; Schumann et al., 2019).

The above results are of significance for lightning protection of tall structures. For example, for a 200-m tall tower (typical of modern wind turbines), located in an area with a yearly ground flash density of about 3 flash/km^2, one would expect using Eriksson's empirical formula [Eriksson, 1987] 3.75 upward flashes, and a total of 37 flashes in the 1.5-km-radius area of around the tower (12.5 km^2). Assuming that on average 7.5% of the flashes are positive [Rakov, 2003] and taking into account that positive flashes tend to exhibit a single return stroke, we would have, out of the 37 flashes in this area, about 3 positive return strokes, which are able to produce fields that are high enough to initiate upward flashes. This reasoning applies if the considered structure is the only one in the area and located on a flat ground. If the tower is located on a mountainous area, the resulting number of upward flashes initiated by nearby positive strokes can be even higher. It is also worth noting that we do not consider the background electric field in this study, the effect of which can be very complex. For example, one could expect in the case when the positive CG flash is close to the tall structure that the cloud charge distribution above the tower creates an opposite field to that created by the return stroke in the positive flash, therefore impeding the initiation of an upward positive leader from the tower. On the other hand, if the return stroke location is far away, it is less likely that the cloud charge distribution above the tower would impede the upward leader initiation. Note also that in the case of the three leader scenarios (I, II and IV), the amplitude of the electric field change will depend strongly on the altitude of the leader above the ground.

It is finally important to note the limitations of both the model used for the field calculation and the simplified corona model. The field calculation is based on an electrostatic assumption, which can be considered as reasonable for the leader processes and the considered distances (see also, [Rubinstein et al. (1995), Rachidi et al. (1997)]). The application of the electrostatic model to the faster RS process is more questionable, even though positive return strokes (considered in this work) are characterized by slower risetimes compared to negative return strokes. Furthermore, we use a fairly simple geometry of horizontal and vertical leaders without taking into account any branching. A more complex leader geometry can be represented with a combination of horizontal and vertical leaders or by discretizing the leader and obtaining numerical solution.

The corona discharge model is based on a simplified spherical electrode representation. As previously noted, the electric fields predicted by such model could overestimate the fields by a factor as high as 2. The criteria for leader and sustained leader development are based on a combination of results obtained by the model and by observations. Some other external parameters, such as the wind speed, atmospheric conditions and the air chemistry might also play a role. We also do not consider electric field changes prior to any specific event.

Despite the above-mentioned limitations, the proposed model can provide a qualitative insight into the mechanisms of upward leader initiation from tall structures. Note finally that the derived electrostatic model is valid for estimating the electric field enhancement in case of both positive and negative upward lightning, while the corona model is based on a positive corona discharge and it is only valid for modeling a negative upward lightning.

6. Summary and Conclusion

We have derived analytical formulas to describe the electrostatic field changes associated with horizontal and vertical leaders. These formulas were then used to evaluate the field in four different scenarios leading to the triggering of an upward flash from a tower, as observed by Schumann et al. (2019). The obtained results indicate that the three scenarios in which the initiation of the upward lightning occurs during the leader propagation phase exhibit similar peak values and risetimes. Scenarios 1 (In-cloud leader) and 4 (CC phase) result in almost the same waveform (see Figure 4 and 9), mainly due to the fact that most of the field at the observation point is due to the closest part of the leader. Scenario 2 (Positive leader approaching the ground) results in a slightly lower field peak compared to scenarios 1 (In-cloud leader) and 4 (CC phase), depending on how far the downward propagating leader is from the observation point. The order of magnitude of the electric field change associated with a 3-km away return stroke is similar to that of a horizontal leader passing above the tower, however with different risetimes.

We then used the criteria for an upward negative leader initiation obtained from a simplified corona model to estimate the minimum height of a tall structure for an upward flash to be initiated. Due to its relatively fast risetimes, the return stroke phase can trigger upward flashes with fields that are about ten times lower than in the case of slower leader propagation processes for a structure of a given height.

It is worth noting that the simplified criteria used to evaluate the initiation of the upward leader can only be used in the case of one linear excitation with respect to time. We have considered only the field change associated with each scenario and disregarded the background electric field, which might have an appreciable effect on the initiation of an upward flash. We can assume that even the cases with less favorable geometrical and electrical properties could trigger an upward flash depending on how close the value of the background electric field was to the value necessary for the so-called self-initiated upward lightning.

The main contributions of this paper can be summarized as follows:

(i) We derived analytical solutions for leader/RS geometries associated with the observed scenarios leading to the initiation of upward flashes from a tall structure. The resulting field enhancement was used in a simplified corona model at the tip of a tall structure.

(ii) The obtained results suggest that it is possible for an upward negative lightning to be triggered by nearby lightning activity, either during a relatively slow leader propagation phase, or after the faster return stroke phase. In most of the analyzed cases, the field change due to nearby lightning activity was high enough to trigger an upward flash from a structure of moderate height, even without the background electric field.

(iii) Slow processes of leader propagation have the fastest risetime and highest amplitude as the leader is passing just above the observation point since the tangential component of the speed with respect to the ground surface is at its maximum and the distance to the leader is at its minimum.

(iv) Nearby return strokes with relatively fast risetimes (some tens of microseconds) are able to trigger upward negative flashes even for field enhancements about ten times lower than in the case of slower leader propagation processes (risetime of some tens of milliseconds).

(v) The obtained results suggest that electric fields in the order of only 1 kV/m from nearby positive return strokes can potentially initiate an upward flash from a 100-m tall structure. Such field intensities are typical of return strokes at distances as large as a few kilometers.

7. Appendix: Derivation of the fields associated with the 4 scenarios leading to the initiation of an upward lightning from a tall structure.

7.1 Horizontal Leader

Let us start with the derivation of the electric field of a horizontal line charge above a perfectly conducting ground (PCG) as shown in Figure 14a. The electric potential of an arbitrary charge distribution at a given point (x,y) in free space can be calculated as:

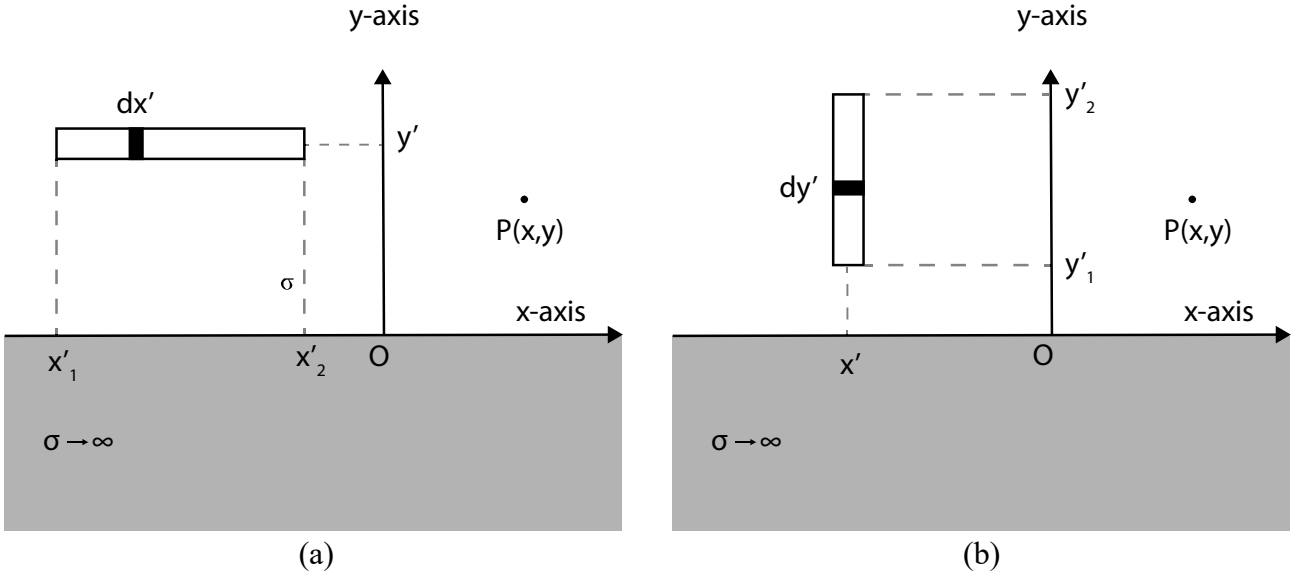

Figure A.1. Geometry of problem. Leader above a perfectly conducting ground. a) Horizontal leader b) Vertical leader. The leader channel radius is assumed to be infinitesimally small.

$$V = \frac{1}{4\pi\varepsilon_0}\int \frac{dq}{r} \tag{A.1}$$

In the case of a horizontal linear charge density λ, (1) can be expressed as:

$$V_H(x,y) = \frac{1}{4\pi\varepsilon_0}\int_{x_1'}^{x_2'} \frac{\lambda(x')dx'}{\sqrt{(x-x')^2+(y-y')^2}} \tag{A.2}$$

Note that y' is constant for a specific geometry of the leader. For the time being, we are ignoring the presence of the perfectly conducting ground. This will be taken into account later using image theory. If we assume a constant linear charge density, the integral in (A.2) can be solved analytically. Note that (A.2) can also be solved analytically for some other simplified charge distributions such as a linear distribution. The solution for a constant linear charge density is:

$$V(x,y) = \frac{-\lambda}{4\pi\varepsilon_0} ln\left(\left|\frac{x-x_2'+\sqrt{(x-x_2')^2+(y-y')^2}}{x-x_1'+\sqrt{(x-x_1')^2+(y-y')^2}}\right|\right) \tag{A.3}$$

Note that the minus sign comes from solving the integral and using the substitution t=x-x'. The components of the electric field can be obtained as follows:

$$\overrightarrow{E_{xH}}(x,y) = -\frac{\partial V(x,y)}{\partial x}\,\widehat{e_x} \tag{A.4}$$

$$\overrightarrow{E_{yH}}(x,y) = -\frac{\partial V(x,y)}{\partial y}\,\widehat{e_y} \qquad \text{(A.5)}$$

Plugging (A.3) into (A.4) and (A.5), we obtain:

$$E_{xH}(x,y) = \frac{\lambda}{4\pi\varepsilon_0}\left(\frac{1}{R_{2H}} - \frac{1}{R_{1H}}\right) = \frac{\lambda}{4\pi\varepsilon_0} f_{1H}(x,y,x_1',x_2',y') \qquad \text{(A.6)}$$

$$E_{yH}(x,y) = \frac{\lambda(y-y')}{4\pi\varepsilon_0}\left(\frac{1}{A_H R_{1H}} + \frac{1}{B_H R_{2H}}\right) = \frac{\lambda(y-y')}{4\pi\varepsilon_0} f_{2H}(x,y,x_1',x_2',y') \qquad \text{(A.7}$$

where f_{1H} and f_{2H} are:

$$f_{1H}(x,y,x_1',x_2',y') = \left(\frac{1}{R_{2H}} - \frac{1}{R_{1H}}\right) \qquad \text{(A.8)}$$

$$f_{2H}(x,y,x_1',x_2',y') = \left(\frac{1}{A_H R_{1H}} + \frac{1}{B_H R_{2H}}\right) \qquad \text{(A.9)}$$

and the coefficients R_{1H}, R_{2H}, A_H and B_H are:

$$R_{1H} = \sqrt{(x-x_1')^2 + (y-y')^2} \qquad \text{(A.10)}$$

$$R_{2H} = \sqrt{(x-x_2')^2 + (y-y')^2} \qquad \text{(A.11)}$$

$$A_H = x - x_1' + R_{1H} \qquad \text{(A.12)}$$

$$B_H = x - x_2' + R_{2H} \qquad \text{(A.13)}$$

Note that (A.12) or (A.13) can be zero in the particular case when

$$y = y' \qquad \text{(A.14)}$$

and when either

$$x - x_1' < 0 \qquad \text{(A.15)}$$

or

$$x - x_2' < 0 \qquad \text{(A.16)}$$

which leads to a field solution tending to infinity. This singularity comes from the fact that the analytical solution of the integral in (A.2) is not defined at points y=y'. Note that this does not impose any limitation to the model since the line charge density is assumed to be infinitely thin, so the singularity can be avoided.

We will now take into account the presence of a perfectly conducting ground. Using image theory, the total electric field at any point with positive *y* coordinate will simply be the sum of the original source and the image source (denoted with the superscript *) with the same charge density of the source but with an opposite polarity.

$$E_{xH\,PCG}(x,y) = E_{xH}(x,y) + E_{xH}{}^{*}(x,y) \qquad \text{(A.17)}$$

$$E_{yH\,PCG}(x,y) = E_{yH}(x,y) + E_{yH}{}^{*}(x,y) \qquad \text{(A.18)}$$

The electric field components of the image source can be readily calculated making the following substitutions in equations (A.6-A.13)

$$\lambda \rightarrow -\lambda \tag{A.19}$$

$$y' \rightarrow -y' \tag{A.20}$$

to take into account the change of charge polarity and the location of the image.

7.2 Vertical Leader

A similar procedure can be followed in the case of a vertical leader shown in Figure A.1b. Note that this is the same problem in free space since only the source has been rotated. The electric field (ignoring the presence of the ground) can be obtained as:

$$E_{xV}(x,y) = \frac{\lambda(x-x')}{4\pi\varepsilon_0}\left(\frac{1}{A_V R_{1V}} + \frac{1}{B_V R_{2V}}\right) = \frac{\lambda(x-x')}{4\pi\varepsilon_0} f_{1V}(x,y,x',y_1',y_2') \tag{A.21}$$

$$E_{yV}(x,y) = \frac{\lambda}{4\pi\varepsilon_0}\left(\frac{1}{R_{2V}} - \frac{1}{R_{1V}}\right) = \frac{\lambda}{4\pi\varepsilon_0} f_{2V}(x,y,x',y_1',y_2') \tag{A.22}$$

where f_{1V} and f_{2V} are:

$$f_{1V}(x,y,x',y_1',y_2') = \left(\frac{1}{A_V R_{1V}} + \frac{1}{B_V R_{2V}}\right) \tag{A.23}$$

$$f_{2V}(x,y,x',y_1',y_2') = \left(\frac{1}{R_{2V}} - \frac{1}{R_{1V}}\right) \tag{A.24}$$

and the coefficients R_{1V}, R_{2V}, A_V and B_V are given by:

$$R_{1V} = \sqrt{(x-x')^2 + (y-y_1')^2} \tag{A.25}$$

$$R_{2V} = \sqrt{(x-x')^2 + (y-y_2')^2} \tag{A.26}$$

$$A_V = y - y_1' + R_{1V} \tag{A.27}$$

$$B_V = y - y_2' + R_{2V} \tag{A.28}$$

Again, the presence of a perfectly conducting ground is accounted for with the use of image theory. The total electric field at any point with positive y coordinate will be the sum of the field from the original source and the field from the image source with the same charge density of the original source but with an opposite polarity:

$$E_{xV\,PCG}(x,y) = E_{xV}(x,y) + E_{xV}{}^*(x,y) \tag{A.29}$$

$$E_{yV\,PCG}(x,y) = E_{yV}(x,y) + E_{yV}{}^*(x,y) \tag{A.30}$$

The electric field components of the image source can be readily calculated from (A.6) and (A.7) making the following substitutions:

$$\lambda \rightarrow -\lambda \tag{A.31}$$

$$y_1' \rightarrow -y_2' \tag{A.32}$$

$$y_2{}' \rightarrow -y_1{}' \tag{A.33}$$

715
716 **7.3 Derivation of the electric field - Scenario 1 (In-cloud leader)**
717
718 Let us derive the electric field as a function of time for the geometry shown in Figure 3a. In order to
719 obtain the time-domain waveform of the electric field, we will consider the leader propagation as a series
720 of electrostatic steps. Defining the points x_1 and x_2 as:
721

$$x_1 = x_0 - v_P t \tag{A.34}$$

$$x_2 = x_0 + v_N t \tag{A.35}$$

722 We can now obtain $E_y(x, y, t)$ from Equation (A.7) for both the positive and the negative leader by
723 setting, for the positive leader:

$$x_1' = x_1 \tag{A.36}$$

$$x_2' = x_0 \tag{A.37}$$

724 and, for the negative leader:

$$x_1' = x_0 \tag{A.38}$$

$$x_2' = x_2 \tag{A.39}$$

725 with:

$$y' = y_0 \tag{A.40}$$

726 for both positive and negative leaders.
727
728 We choose the value of the linear charge density for the positive charge to be:
729

$$\lambda_P = -\frac{v_P}{v_N}\lambda_N \tag{A.41}$$

730 so that the overall net charge along the leader is equal to zero.
731
732 The vertical field at any point (x,y) is then given by:

$$E_{y\,sc1}(x, y, t) = \frac{\lambda_N (y - y_0)}{4\pi\varepsilon_0}\left(f_{2H}(x, y, x_0, x_0 + v_2 t, y_0) - \frac{v_N}{v_P} f_{2H}(x, y, x_0 - v_1 t, x_0, y_0)\right) \tag{A.42}$$

733
734 **7.4 Derivation of the electric field - Scenario 2 (Positive leader approaching the ground)**
735
736 Figure 5a presents the sketch of the second scenario where the positive end of the initially horizontal
737 leader bends toward the ground. We will assume that this happens at a time T_1. The electric field for times
738 smaller than T_1 can be obtained using the expression derived in the previous subsection. The total vertical
739 electric field due to the positive leader can be expressed as

$$E_{y\,sc2}(x, y, t) = \begin{cases} E_{y\,sc1}(t), & t \le T_1 \\ E_{y2}(t), & t > T_1 \end{cases} \tag{A.43}$$

740 At time T_1, the positive leader will reach the coordinate:

$$x_{TD} = x_0 - v_P T_1 \tag{A.44}$$

741 The negative part of the leader will be treated as in previous section. The field due to the positive part of

the leader in the vertical channel will be given by Equation (A.22) with:

$$x' = x_{T_1} \tag{A.45}$$

$$y_1' = y_0 - v_P(t - T_1) \tag{A.46}$$

$$y_2' = y_0 \tag{A.47}$$

Finally, the electric field E_{y2} can be obtained as:

$$E_{y2}(x,y,t) = \frac{\lambda_N (y - y_0)}{4\pi\varepsilon_0}\left(f_{2H}(x,y,x_0,x_0 + v_2 t, y_0) - \frac{v_N}{v_P} f_{2H}(x,y,x_0 - v_1, T_1, x_0, y_0)\right) - \frac{\lambda_N v_N}{4\pi\varepsilon_0 v_P} f_{2V}(x,y,x_{T_1}, y_0 - v_P(t - T_1)) \tag{A.48}$$

7.5 Derivation of the electric field - Scenario 3 (Positive RS)

The return stroke is represented by a negative line charge propagating upward from the ground to the initiation point as shown in Figure 7a with the same line charge density as in the preceding downward positive leader but with an opposite sign. The vertical electric field due to the return stroke is given by:

$$E_{y\,sc3}(x,y,t) = \begin{cases} E_{y1}(t), & t \le T_2 \\ E_{y2}(t) = E_{y1}(T_2) + E_{y2}{}'(t), & t > T_2 \end{cases} \tag{A.49}$$

where T_2 is the time when the return stroke front reaches the maximum height y_0 given by:

$$T_2 = \frac{y_0}{v_{RS}} \tag{A.50}$$

$E_{y1}(t)$ can be calculated using equation (A.22) with the following substitutions:

$$x' = x_{RS} \tag{A.51}$$

$$y_1' = 0 \tag{A.52}$$

and:

$$y_2' = v_{RS} t \tag{A.53}$$

We obtain:

$$E_{y1}(x,y,t) = -\frac{\lambda_P}{4\pi\varepsilon_0} f_{2V}(x,y,x_{RS},0,v_{RS}t) \tag{A.54}$$

where the negative sign is due to the fact that the positive return stroke is neutralizing positive charges along the channel.

After the return stroke front reaches the maximum altitude, the contribution of the horizontal part can be taken into account by plugging the following expressions

$$x_1' = x_{RS} \tag{A.55}$$

$$x_2' = x_{RS} + v_{RS}(t - T_2) \tag{A.56}$$

$$y' = y_0 \tag{A.57}$$

into Equation (A.7), which yields

$$E_{y2}(x,y,t) = -\frac{\lambda_P}{4\pi\varepsilon_0}\left(f_{2V}(x,y,x_{RS},0,v_{RS}T_2) + (y-y_0)f_{2H}(x,y,x_{RS},x_{RS}+v_{RS}(t-T_2),y_0)\right) \quad \text{(A.58)}$$

7.6 Derivation of the electric field - Scenario 4 (CC phase)

To evaluate the electric field associated with Scenario 4 illustrated in Figure 9a, we can use again Equation (A.7) with the following parameters:

$$x_1' = x_0 \quad \text{(A.59)}$$

$$x_2' = v_N t \quad \text{(A.60)}$$

with:

$$y' = y_0 \quad \text{(A.61)}$$

The final expression can be straightforwardly obtained as:

$$E_{y\,sc4}(x,y,t) = \frac{\lambda_N(y-y_0)}{4\pi\varepsilon_0} f_{2H}(x,y,x_0,x_0+v_N t,y_0) \quad \text{(A.62)}$$

8. Acknowledgment

This work was supported in part by the Swiss National Science Foundation (Project No. 200020_175594). The source code for the analytical solutions can be found online at https://github.com/IToni93/other_triggered_lightning_analytical.git [Sunjerga et al. (2020b)]. An interactive interface can also be found at https://IToni93.github.io/other_triggered_lightning_analytical/. We would like to thank Prof. Marcelo Saba and two anonymous reviewers for their careful review of our manuscript and their many insightful comments and suggestions that helped us improve the quality of the paper.

9. References

Aleksandrov, N. L., Bazelyan, E. M., Carpenter, R. B., Jr, Drabkin, M. M., & Raizer, Y. P. (2001). The effect of coronae on leader initiation and development under thunderstorm conditions and in long air gaps. Journal of Physics D: Applied Physics, 34(22), 3256–3266. https://doi.org/10.1088/0022-3727/34/22/309

Aleksandrov, N. L., Bazelyan, E. M., Drabkin, M. M., Carpenter, R. B., Jr., & Raizer, Y. P. (2002). Corona discharge at the tip of a tall object in the electric field of a thundercloud. Plasma Physics Reports, 28(11), 953–964. https://doi.org/10.1134/1.1520289

Arcanjo, M., Mazala, K., Guimaraes, M., & Visacro, S. (2018). Estimating the electric field above the top of grounded structures upon UCL initiation in CG lightning from close E-field measured over the ground. 2018 34th International Conference on Lightning Protection (ICLP). Presented at the 2018 34th International Conference on Lightning Protection (ICLP). https://doi.org/10.1109/iclp.2018.8503316

Bazelyan E M and Raizer Yu P 1998 Spark Discharge (Boca Raton, FL: CRC Press)

Bazelyan E M and Raizer Yu P 2000 Lightning Physics and Lightning Protection (Bristol: IOPP)

Berger, K., and E. Vogelsanger (1969), New results of lightning observations, in Planeteary Electrodynamics, edited by S. C. Coroniti and J. Hughes, pp. 498 – 510, Gordon and Breach, New York.

Campos Z.S et al. Does the average downward speed of a lightning leader change as it approaches the ground? – An observational approach. Vaisala 2010 International. Conferences on Lightning.

Campos, L. Z. S., M. M. F. Saba, T. A. Warner, O. Pinto Jr., E. P. Krider, and R. E. Orville (2014), High-speed video observations of natural cloud-to-ground lightning leaders - A statistical analysis, Atmos. Res., 135-136, 285-305, doi:10.1016/j.atmosres.2012.12.011.

Chauzy, S., & Rennela, C. (1985). Computed response of the space charge layer created by corona at ground level to external electric field variations beneath a thundercloud. Journal of Geophysical Research, 90(D4), 6051. https://doi.org/10.1029/jd090id04p06051

Cooray, V. (1995). A model for positive return strokes Inst. Phys. Conf. Ser., 143 , pp. 363-371

Cooray, V. (2000). The modelling of positive return strokes in lightning flashes. Journal of Atmospheric and Solar-Terrestrial Physics, 62(3), 169–187. https://doi.org/10.1016/s1364-6826(99)00056-5

Cooray, V. (2003). The Lightning Flash.

Eriksson, A. J. (1987). The Incidence of Lightning Strikes to Power Lines. IEEE Transactions on Power Delivery, 2(3), 859–870. https://doi.org/10.1109/tpwrd.1987.4308191Gallimberti I 1979 J. Physique 40 C7 193

Gao, Y., Chen, M., Lyu, W., Qi, Q., Qin, Z., Du, Y., & Zhang, Y. (2020). Leader Charges, Currents, Ambient Electric Fields, and Space Charges Along Downward Positive Leader Paths Retrieved From Ground Measurements in Metropolis. Journal of Geophysical Research: Atmospheres, 125(19). https://doi.org/10.1029/2020jd032818

Kasemir, H. W. (1960). A contribution to the electrostatic theory of a lightning discharge. Journal of Geophysical Research, 65(7), 1873–1878. https://doi.org/10.1029/jz065i007p01873

Lin, Y. T., Uman, M. A., Tiller, J. A., Brantley, R. D., Beasley, W. H., Krider, E. P., & Weidman, C. D. (1979). Characterization of lightning return stroke electric and magnetic fields from simultaneous two-station measurements. Journal of Geophysical Research, 84(C10), 6307. https://doi.org/10.1029/jc084ic10p06307

Meek J M and Craggs I D 1978 Electrical Breakdown of Gases (New York: Wiley)

Montanyà J. Turbines shoot upside-down lightning. (2014). Nature, 506(7488), 268–268. https://doi.org/10.1038/506268a

Proctor, D. E. (1997). Lightning flashes with high origins. Journal of Geophysical Research: Atmospheres, 102(D2), 1693–1706. https://doi.org/10.1029/96jd02635

Rachidi, F., Rubinstein, M., Guerrieri, S., & Nucci, C. A. (1997). Voltages induced on overhead lines by dart leaders and subsequent return strokes in natural and rocket-triggered lightning. IEEE Transactions on Electromagnetic Compatibility, 39(2), 160–166. https://doi.org/10.1109/15.584939

Rachidi, F., Janischewskyj, W., Hussein, A. M., Nucci, C. A., Guerrieri, S., Kordi, B., & Jen-Shih Chang. (2001). Current and electromagnetic field associated with lightning-return strokes to tall towers. IEEE Transactions on Electromagnetic Compatibility, 43(3), 356–367. https://doi.org/10.1109/15.942607

Rachidi, F., Rubinstein, M., Montanya, J., Bermudez, J.-L., Rodriguez Sola, R., Sola, G., & Korovkin, N. (2008). A Review of Current Issues in Lightning Protection of New-Generation Wind-Turbine Blades. IEEE Transactions on Industrial Electronics, 55(6), 2489–2496. https://doi.org/10.1109/tie.2007.896443

Rakov, V. A. (2003). A Review of Positive and Bipolar Lightning Discharges. Bulletin of the American Meteorological Society, 84(6), 767–776. https://doi.org/10.1175/bams-84-6-767

Rakov, V. A., & Uman, M. A. (2003). Lightning: Physics and effects. Cambridge, U.K: Cambridge University Press.

Rubinstein, M., Zuber, J., Smorgonskiy, A., Rachidi, F., & Diendorfer, G. (2016, September). Correlation vs. causality in other-triggered upward lightning in tower flashes. 2016 33rd International Conference on Lightning Protection (ICLP). 2016 33rd International Conference on Lightning Protection (ICLP). https://doi.org/10.1109/iclp.2016.7791360

Saba, M. M. F., Schumann, C., Warner, T. A., Ferro, M. A. S., de Paiva, A. R., Helsdon, J., Jr, & Orville, R. E. (2016). Upward lightning flashes characteristics from high-speed videos. Journal of Geophysical Research: Atmospheres, 121(14), 8493–8505. https://doi.org/10.1002/2016jd025137

Schumann, C., Saba, M. M. F., Warner, T. A., Ferro, M. A. S., Helsdon, J. H., Jr., Thomas, R., & Orville, R. E. (2019). On the Triggering Mechanisms of Upward Lightning. Scientific Reports, 9(1). https://doi.org/10.1038/s41598-019-46122-x

Shen, Y., Chen, M., Du, Y., & Dong, W. (2019). Line Charge Densities and Currents of Downward Negative Leaders Estimated From VHF Images and VLF Electric Fields Observed at Close Distances.

IEEE Transactions on Electromagnetic Compatibility, 61(5), 1507–1514. https://doi.org/10.1109/temc.2018.2864199

Singer, H., Steinbigler, H., & Weiss, P. (1974). A Charge Simulation Method for the Calculation of High Voltage Fields. IEEE Transactions on Power Apparatus and Systems, PAS-93(5), 1660–1668. https://doi.org/10.1109/tpas.1974.293898

Smorgonskiy, A., Rachidi, F., Rubinstein, M., Diendorfer, G., & Schulz, W. (2011). On the proportion of upward flashes to lightning research towers. 2011 7th Asia-Pacific International Conference on Lightning. Presented at the 2011 7th Asia-Pacific International Conference on Lightning (APL). https://doi.org/10.1109/apl.2011.6110248

Smorgonskiy, A., Tajalli, A., Rachidi, F., Rubinstein, M., Diendorfer, G., & Pichler, H. (2015a). An analysis of the initiation of upward flashes from tall towers with particular reference to Gaisberg and Säntis Towers. Journal of Atmospheric and Solar-Terrestrial Physics, 136, 46–51. https://doi.org/10.1016/j.jastp.2015.06.016

Smorgonskiy, A., Egüz, E., Rachidi, F., Rubinstein, M., & Cooray, V. (2015b). A model for the evaluation of the electric field associated with the lightning-triggering rocket wire and its corona. Journal of Geophysical Research: Atmospheres, 120(20), 10,964-10,973. https://doi.org/10.1002/2015jd023373

Soriano, L. R., & de Pablo, F. (2007). Total flash density and the intracloud/cloud-to-ground lightning ratio over the Iberian Peninsula. Journal of Geophysical Research: Atmospheres, 112(D13), n/a-n/a. https://doi.org/10.1029/2006jd007624

Stock, M. G., Krehbiel, P. R., Lapierre, J., Wu, T., Stanley, M. A., & Edens, H. E. (2017). Fast positive breakdown in lightning. Journal of Geophysical Research: Atmospheres, 122(15), 8135–8152. https://doi.org/10.1002/2016jd025909

Sunjerga, A., Mostajabi, A., Rachidi, F., Pineda, N., Romero, D., Van der Velde, O. A., … Diendorfer, G. (2018). On the Classification of Self-Triggered versus OtherTriggered Lightning Flashes. 2018 34th International Conference on Lightning Protection (ICLP). Presented at the 2018 34th International Conference on Lightning Protection (ICLP). https://doi.org/10.1109/iclp.2018.8503322

Sunjerga, A., Rubinstein, M., Pineda, N., Mostajabi, A., Azadifar, M., Romero, D., … Rachidi, F. (2020a). LMA observations of upward lightning flashes at the Säntis Tower initiated by nearby lightning activity. Electric Power Systems Research, 181, 106067. https://doi.org/10.1016/j.epsr.2019.106067

Sunjerga, A., Rubinstein, M., Rachidi, F., & Cooray, V. (2020b). On the Initiation of Upward Negative Lightning by Nearby Lightning Activity: An Analytical Approach - Source Code (v1.0.0) [Computer software]. Zenodo. https://doi.org/10.5281/ZENODO.4321780

Uman M A 1987 The Lightning Discharge (New York: Academic)

van der Velde, O. A., & Montanyà, J. (2013). Asymmetries in bidirectional leader development of lightning flashes. Journal of Geophysical Research: Atmospheres, 118(24), 13,504-13,519. https://doi.org/10.1002/2013jd020257

Wang, D., Takagi, N., Watanabe, T., Sakurano, H., & Hashimoto, M. (2008). Observed characteristics of upward leaders that are initiated from a windmill and its lightning protection tower. Geophysical Research Letters, 35(2). https://doi.org/10.1029/2007gl032136

Warner, T. A., Cummins, K. L., & Orville, R. E. (2012). Upward lightning observations from towers in Rapid City, South Dakota and comparison with National Lightning Detection Network data, 2004-2010. Journal of Geophysical Research: Atmospheres, 117(D19), n/a-n/a. https://doi.org/10.1029/2012jd018346

Wooi, C.-L., Abdul-Malek, Z., Salimi, B., Ahmad, N. A., Mehranzamir, K., & Vahabi-Mashak, S. (2015). A Comparative Study on the Positive Lightning Return Stroke Electric Fields in Different Meteorological Conditions. Advances in Meteorology, 2015, 1–12. https://doi.org/10.1155/2015/307424